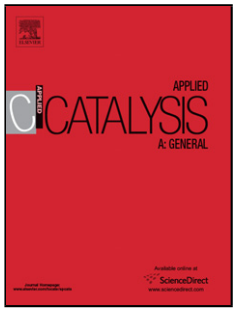

Title: Synthesis of Glycerol Carbonate from Urea and Glycerol Using Polymer-supported Metal Containing Ionic Liquid Catalysts

Author: Dong-Woo Kim Kyung-Ah Park Min-Ji Kim Dong-Heon Kang Jeong-Gyu Yang Dae-Won Park

PII: S0926-860X(13)00776-X
DOI: http://dx.doi.org/doi:10.1016/j.apcata.2013.12.032
Reference: APCATA 14631

To appear in: *Applied Catalysis A: General*

Received date: 1-11-2013
Revised date: 11-12-2013
Accepted date: 23-12-2013

Please cite this article as: D.-W. Kim, K.-A. Park, M.-J. Kim, D.-H. Kang, J.-G. Yang, D.-W. Park, Synthesis of Glycerol Carbonate from Urea and Glycerol Using Polymer-supported Metal Containing Ionic Liquid Catalysts, *Applied Catalysis A, General* (2014), http://dx.doi.org/10.1016/j.apcata.2013.12.032

*Graphical Abstract (for review)

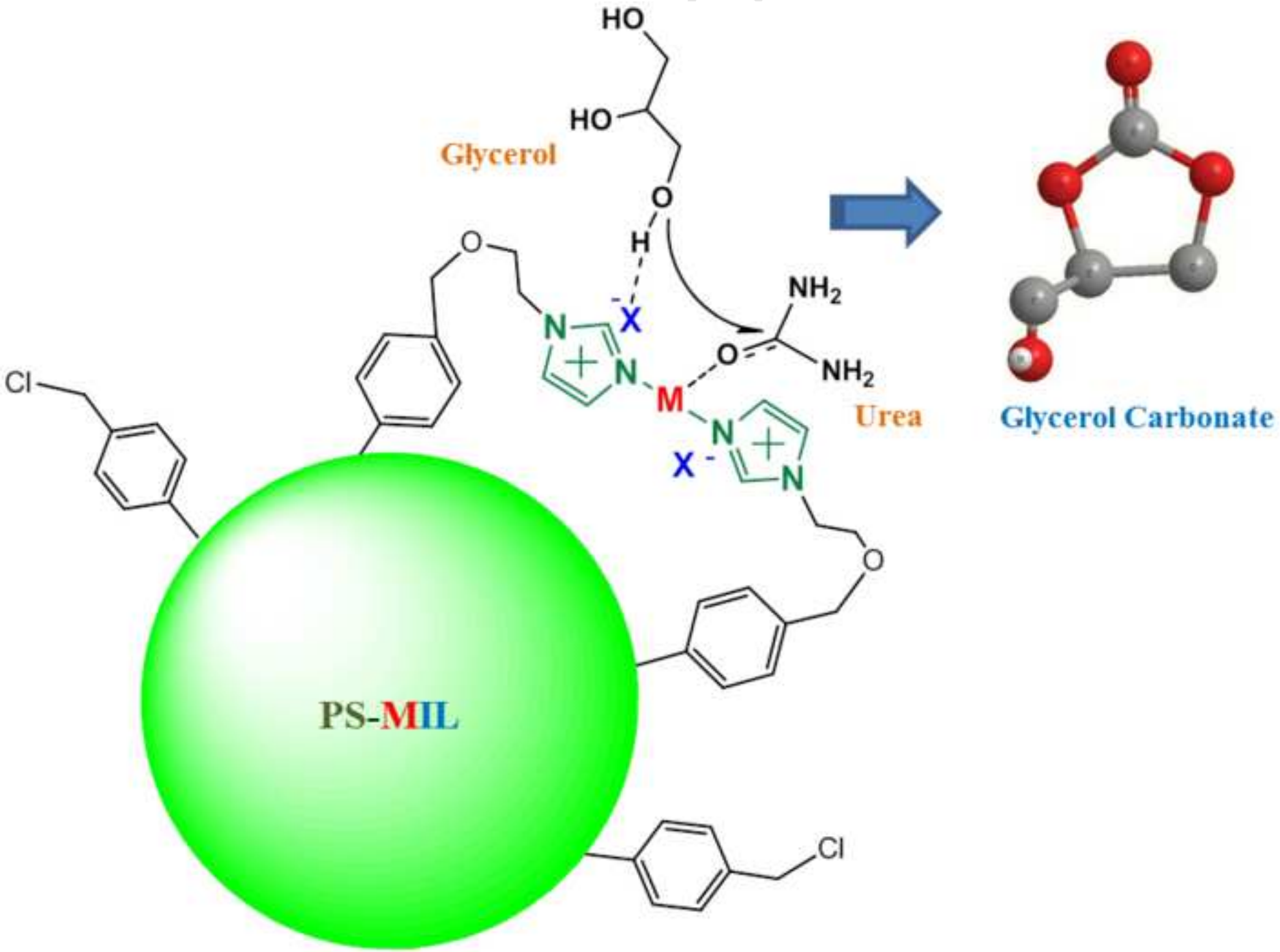

Highlights

- The polystyrene-supported metal containing ionic liquid catalysts were successfully synthesized.
- PS-$(Im)_2ZnI_2$ with well-balanced acid-base properties exhibited high catalytic activity.
- The reaction pathway was studied via FT-IR and ^{13}C NMR.
- PS-$(Im)_2ZnI_2$ was easily recovered and reused.

Synthesis of Glycerol Carbonate from Urea and Glycerol Using Polymer-supported Metal Containing Ionic Liquid Catalysts

Dong-Woo Kim, Kyung-Ah Park, Min-Ji Kim, Dong-Heon Kang, Jeong-Gyu Yang, and Dae-Won Park*

School of Chemical and Biomolecular Engineering, Pusan National University, Busan 609-735, Republic of Korea

**Corresponding author: dwpark@pusan.ac.kr*

ABSTRACT

Polystyrene-supported, metal containing imidazolium salt [PS-$(Im)_2MX_2$] catalysts were prepared and characterized by various analytical methods, and their role in the synthesis of glycerol carbonate from glycerol and urea was investigated under mild conditions. Among different metal containing PS-$(Im)_2MBr_2$ catalysts, the yield of GC increased Cu < Mg < Zn, which is the order of acid-base balance of the catalysts. PS-$(Im)_2ZnI_2$ catalyst, which showed a good balance of the acid-base properties, was the most active and selective catalyst; it was readily recoverable and reusable in the subsequent reaction cycles. Furthermore, the reaction pathway for the glycerolysis of urea was studied with the time-on-line analysis of the products *via* a combination of FT-IR spectroscopy and ^{13}C NMR analysis. The effects of reaction parameters such as temperature, degree of vacuum, catalyst loading, and the ratio of reactants on the reactivity were also investigated to elucidate the reaction mechanism.

Keywords: Glycerol carbonate, Glycerol, Urea, Polymer Support, Ionic liquid.

* Corresponding author. Tel.: +82 51 510 2399; fax: +82 51 512 8563.
E-mail address: dwpark@pusan.ac.kr

1. Introduction

Since the last decade, biodiesel has gained increasing importance as a diesel-engine fuel for because it is renewable and clean **[1-3]**. Because of the rapid increase in the use of biodiesel and the sharp decrease in the price of glycerol (a by-product generated with the amount at one tenth of biodiesel production), glycerol can become a major platform chemical and has been identified as an important building block for future biorefineries by the DOE **[4]**.

Among the chemicals derived from glycerol, glycerol carbonate (4-hydroxymethyl-1,3-dioxolan-2-one; GC) has been relatively recently introduced to the chemical industry and has been recognized to have extensive potential applicability **[5-9]**. Moreover, inexpensive GC could serve as a source of new polymeric materials such as glycidol, which is a high-value component in the production of a number of polymers **[9,10]**. The high functionality of glycidol, along with the versatile and well-investigated reactivity of its hydroxyl groups, has led to the formation of a number of derivatives. Indeed, many polyglycerols have been commercialized for applications ranging from cosmetics to controlled drug release **[11]**.

GC is conventionally synthesized *via* typical protocols used for other low-molecular-weight organic carbonates. Transesterification of glycerol can be readily performed with dimethyl carbonate **[12]**, ethylene carbonate **[13]**, or propylene carbonate **[14]**. The carbonates utilized during the transesterification process are typically generated by utilizing phosgene or by means of energy-intensive routes employing epoxides. However, the reaction of glycerol with phosgene is limited by the toxic and environmentally hazardous nature of phosgene. Although there are some reports on the direct carbonylation of glycerol with carbon dioxide using tin complexes, the applicability of such processes is hampered by serious limitations such as unfavorable thermodynamic equilibrium and low yields **[15]**.

An alternative synthesis method for GC is the glycerolysis of urea, a reaction that has been recently developed **[16-18]**. Its main advantage is that the reactants, glycerol and urea, are inexpensive, easily available, and neither explosive nor poisonous. In addition, the ammonia generated in the synthesis of GC from urea and glycerol can easily be converted back to urea by reaction with carbon dioxide.

Much effort has been devoted to the search for effective catalysts for the glycerolysis of urea. Homogeneous catalysis employing inorganic salts such as $ZnSO_4$ **[19]**, $MgSO_4$ **[20]**, and ZnO **[21]** has been described, and recently, certain heterogeneous systems based on these oxides have also been reported **[22,23]**.

Polymer-supported catalysts are extensively used in both industry and academia because of the advantages they offer compared to homogeneous catalysts **[24-26]**. Recently, polymer-supported ionic liquids have been exploited as heterogeneous catalysts in the synthesis of cyclic carbonates, and were found to offer the dual features of a homogeneous ionic liquid and heterogeneous catalyst. Compared to pure ILs, such heterogeneous catalysts have additional advantages such as facilitating the reduction of the amount of ILs employed, recovery of the catalyst from the reaction mixture, and ease of separation **[27-29]**.

These data and the results of other prior studies **[30,31]** suggest that the catalysts for the reaction between glycerol and urea should possess both acidity and basicity to be effective, and also that there is a subtle balance between the acidity and basicity of such catalysts. In particular, the Lewis-acid sites activate the carbonyl group of urea whereas the Lewis-base sites activate the hydroxyl groups of glycerol **[13,16,32]**.

In our previous work **[33]**, the glycerolysis of urea was evaluated using metal containing ionic liquid (MIL) as efficient catalyst. However, the homogeneous system of

MIL catalysts showed poor catalyst separation. The exploration of heterogeneous catalysts that are highly efficient under mild reaction conditions still remains a challenge. This paper reports the preparation of structurally modified polystyrene based on a Merrifield peptide resin supported metal containing imidazolium salt [PS-$(Im)_2MX_2$] and its characterization *via* various physicochemical methods. The catalytic performance of PS-$(Im)_2MX_2$ in the synthesis of GC from glycerol and urea is investigated. To improve the understanding of the reaction pathway and mechanism, the influence of the acid-base properties of the PS-$(Im)_2MX_2$ catalyst on the synthesis of GC is evaluated. In addition, the effects of the reaction time, reaction temperature, degree of vacuum, and catalyst loading are discussed. The PS-$(Im)_2MX_2$ catalyst was subjected to a recycle test in order to examine its stability.

2. Experimental

2.1. Materials

High-purity (>99%) 1-(2-hydroxyethyl)imidazole, metal halides ($ZnCl_2$, $ZnBr_2$, ZnI_2, $MgBr_2$, and $CuBr_2$), and Merrifield's peptide resin (MPR, 1% divinylbenzene, 4.0 mmol Cl/g) were purchased from Sigma-Aldrich. Glycerol (>99%), urea (>99%), GC (>99 %), and methanol (>99 %) were also obtained from Sigma-Aldrich. All materials were used without further purification.

2.2. Synthesis of polystyrene-supported metal containing imidazolium salt catalyst

The synthesis of PS-$(Im)_2MX_2$ was carried out *via* two steps (Scheme 1). First, bis[1-(2-hydroxyethyl) imidazolium]metal halide, $(HIm)_2MX_2$, was synthesized by metal insertion **[33,34]** using an ethanol solution (100 mL) containing 1-(2-hydroxyethyl)imidazole (40

mmol) that was added to an ethanolic solution (100 mL) of the metal halide (20 mmol). This mixture was stirred for 2 h at 50 °C and subsequently filtered. A crystalline solid was obtained after drying at 100 °C for 24 h under vacuum.

$(HIm)_2MX_2$ was immobilized on polystyrene by alkoxylation as per our previous report **[30,35]**. A mixture of MPR (5 g), $(HIm)_2MX_2$ (10 mmol), and acetonitrile (100 mL) was heated at 80 °C for 48 h in a 250-mL round-bottomed flask equipped with a condenser. After cooling the reaction mixture to room temperature, the solid was collected by filtration and washed several times with ethanol. The collected solid was dried at 80 °C for 24 h under vacuum. The supported catalysts were denoted PS-$(Im)_2ZnI_2$, PS-$(Im)_2ZnBr_2$, PS-$(Im)_2ZnCl_2$, PS-$(Im)_2MgBr_2$, and PS-$(Im)_2CuBr_2$, corresponding to the metal halides employed.

2.3. Characterization of PS-MIL catalyst

Elemental analysis (EA) of the samples was carried out using a Vario EL III instrument. The samples (2 mg) were heated to 1100 °C and sulfanilic acid was used as a standard. The Fourier transform infrared (FT-IR) spectra were acquired on an AVATAR 370 Thermo Nicolet spectrophotometer with a resolution of 4 cm^{-1}. The textural properties of the samples were analyzed by recording the N_2 adsorption isotherm at 77 K, using a BET apparatus (Microneritics ASAP 2020). Before gas sorption analysis, the samples were pretreated for 12 h at 120 ^oC under vacuum. The X-ray photoelectron spectroscopy (XPS) of the catalysts was conducted with the Theta Probe AR-XPS System X-ray source using monochromated Al Kα radiation ($h\nu$ = 1486.6 eV). Thermogravimetric analysis (TGA) was performed from room temperature to 500 °C on an AutoTGA 2950 apparatus under a nitrogen flow of 100 mL min^{-1} at a heating rate of 10 °C min^{-1}. The scanning electron

microscopy (SEM) micrographs were acquired with a Hitachi S-47000 microscope operated at 30 kV. CO_2 and NH_3 temperature-programmed-desorption (TPD) profiles were acquired using a chemisorption analyzer (BEL-CAT) as follows: prior to measurements, 0.1 g of the sample was activated in He (30 mL/min) at 280 °C for 1 h. The sample was subsequently exposed to the pulses of CO_2 (10%) or NH_3 (10%) in He at 40 °C for 1 h. The sample was then flushed with He (30 mL/min) for 1 h. TPD measurements were carried out by raising the temperature from 40 to 300 °C at a heating rate of 5 °C/min.

2.4. Synthesis of glycerol carbonate from glycerol and urea

The synthesis of GC *via* the reaction of glycerol with urea was carried out in a 50-mL glass reactor equipped with a magnetic stirrer and condenser (Scheme 2). In a typical reaction run, the catalyst, glycerol, and urea were charged into the reactor. When the desired temperature was attained, the reaction was initiated by stirring under vacuum to remove ammonia as a by-product. The products and reactants were analyzed using a gas chromatograph (HP 6890N) equipped with an FID and a capillary column (HP-INNOWAX, polyethylene glycol). Tetraethylene glycol (TEG) was used as the internal standard. The conversion and selectivity were calculated based on the assumption that glycerol was the limiting reactant. In addition to determining the by-products and intermediates, the reaction mixture was analyzed *via* FT-IR (AVATAR 370 Thermo Nicolet spectrophotometer with a resolution of 4 cm^{-1}) and ^{13}C-NMR (Varian 500 MHz, CD_3OD).

3. Results and discussion

3.1. Characterization of catalysts

The successful covalent immobilization of the metal containing imidazolium salt on the surface of the polystyrene support was confirmed using FT-IR spectroscopy (Fig. 1). In the FT-IR spectral analyses of PS-$(Im)_2MX_2$ and MPR, the characteristic peak corresponding to the stretching frequency of the CH_2Cl functional group (1265 cm^{-1}) disappeared in each spectra of the PS-$(Im)_2MX_2$ series, suggesting the complete modification of MPR **[27-29]**. Four new peaks were observed for PS-$(Im)_2MX_2$ in the regions 1610, 1560, 1145, and 1070 cm^{-1}, which were absent from the MPR spectrum; these peaks are associated with the stretching frequencies of the imidazolium ring **[36]**.

The XPS analysis of PS-$(Im)_2MX_2$ was used to confirm the structure of the catalysts. The N 1s spectra of PS-$(Im)_2MX_2$ are presented in Fig. 2. The spectra of all of the PS-$(Im)_2MX_2$ catalysts exhibited the characteristic peak of the imidazolium nitrogen at 401.7 eV **[37-40]**. Moreover, the Cl 2p, Br 3d, and I 3d spectra of PS-$(Im)_2MX_2$ were acquired to identify the bonding nature of the halogen associated with the metal species, as illustrated in the supporting informations (Fig. S1, S2, S3). The Cl 2p spectrum of PS-$(Im)_2ZnCl_2$ (Fig. S1) showed a peak near 197.5 eV, confirming that the bonds between chlorine and zinc are ionic, and not covalent **[37]**. The Br 3d spectrum of PS-$(Im)_2MBr_2$ showed a peak at *ca*. 68 eV (Fig. S2), which is assigned to negatively charged bromide ion **[41]**. An I 3d peak was observed at 619.3 eV in the case of PS-$(Im)_2ZnI_2$ (Fig. S3), which indicated the anionic state of iodine **[41,42]**. The aforementioned results are a clear indication of the successful immobilization of metal containing imidazolium salt on the support, as shown in Scheme 2.

The content of metal containing imidazolium salt in the PS-$(Im)_2MX_2$ samples was analyzed by elemental analysis; the amount of immobilized $(Im)_2MX_2$ in the catalysts is summarized in Table 1. The amount of $(Im)_2MX_2$ immobilized on the polystyrene support varied from 0.60 to 0.89 mmol/g-cat meaning that about 50% of the MPR surface was

substituted by the $(Im)_2MX_2$. The specific surface area of PS-$(Im)_2ZnI_2$ was measured by N_2 adsorption-desorption isotherm behavior (BET) and was found to be 1.95 m^2/g. The pore volume and average pore size of PS-$(Im)_2ZnI_2$ were 0.0013 cm^3/g and 3.2 nm, respectively. However, the original MPR has BET area 0.44 m^2/g with average pore diameter of 16.1 nm. The thermogravimetric analysis (TGA) curves of the PS-$(Im)_2MX_2$ catalysts were shown in Fig. 3; the first weight loss around 100 °C resulted from the removal of absorbed water molecules. The further weight loss occurring between 200 and 400 °C was likely due to the decomposition of the $(Im)_2MX_2$ on the surface of polystyrene resin, and then the structure of polystyrene resin was collapsed over 400 °C. The results demonstrate that all of the PS-$(Im)_2MX_2$ samples showed good thermal stability up to 300 °C, which is much higher than the reaction temperature for the synthesis of GC from glycerol and urea. The SEM images of the polystyrene support and PS-$(Im)_2ZnI_2$ are presented in Fig. 4. The images show that the diameter of the polymer beads was approximately 70 μm and the spherical shape of the beads was retained even after immobilization.

The differences in the acidic and basic properties of the PS-$(Im)_2MX_2$ catalysts was evaluated based on the temperature programmed desorption (TPD) of HN_3 and CO_2, respectively. The results of the TPD characterization of the catalysts are summarized in Table 2 and illustrated in Fig. S4 and S5. Fig S4 shows the CO_2-TPD profiles of the various PS-$(Im)_2MX_2$ catalysts, and the distribution of the basic sites of different strengths was estimated as follows: weak groups, 323–423 K; and medium-to-strong groups, 425–573 K **[43,44]**. Based on the results presented in Table 2, it can be concluded that the PS-$(Im)_2ZnI_2$ catalyst possessed significantly high basicity compared to the catalysts with Br^- and Cl^- anions, which is in accordance with the increasing nucleophilicity of the anion. On the other hand, in the presence of the bromide anion, the PS-$(Im)_2MBr_2$ catalysts possessing different metal ions

showed similar basicity. Based on Table 2, the basicity sequence can be derived as follows: PS-$(Im)_2ZnI_2$ (6.67 mmol/g) ≫ PS-$(Im)_2MgBr_2$ (3.92 mmol/g) ≈ PS-$(Im)_2CuBr_2$ (3.80 mmol/g) ≈ PS-$(Im)_2ZnBr_2$ (3.79 mmol/g) > PS-$(Im)_2ZnCl_2$ (2.01 mmol/g). The NH_3-TPD profiles of the PS-MIL catalysts are shown in Fig. S5; it shows that the acidity can be classified into two groups **[43]**: weak-to-medium groups, 323–523 K; and strongly acidic groups, 473–573 K. Based on the data in Table 2, it can be concluded that PS-$(Im)_2CuBr_2$ exhibited the highest acidity and the order of acidity was: PS-$(Im)_2CuBr_2$ (41.90 mmol/g) ≫ PS-$(Im)_2MgBr_2$ (14.89 mmol/g) > PS-$(Im)_2ZnI_2$ (6.01 mmol/g) > PS-$(Im)_2ZnCl_2$ (5.85 mmol/g) > PS-$(Im)_2ZnBr_2$ (4.18 mmol/g). In addition, the ratio of acid/base sites was as follows: PS-$(Im)_2ZnI_2$ (0.9), PS-$(Im)_2ZnBr_2$ (1.1), PS-$(Im)_2ZnCl_2$ (2.9), PS-$(Im)_2MgBr_2$ (3.8), and PS-$(Im)_2CuBr_2$ (11.1). PS-$(Im)_2ZnI_2$ and PS-$(Im)_2ZnBr_2$ have a quite good balance of acid-base sites, but PS-$(Im)_2CuBr_2$ has very high acid/base ratio.

Moreover, the acidity and basicity of the catalysts was evaluated based on the Knoevenagel condensation reaction **[45]** between malononitrile and benzaldehyde, which is typically catalyzed by basic sites, and the acetalization **[46]** of benzaldehyde with ethanol, which is a reaction catalyzed purely by acid sites. The results of the initial reaction rates of the Knoevenagel condensation and acetalization using catalysts with different acid–base pairs are presented in Fig. 5. The basicity of the catalysts showed the order: PS-$(Im)_2ZnI_2$ > PS-$(Im)_2ZnBr_2$ ≈ PS-$(Im)_2MgBr_2$ ≈ PS-$(Im)_2CuBr_2$ > PS-$(Im)_2ZnCl_2$. On the other hand, the order of activity was as follows: PS-$(Im)_2CuBr_2$ ≫ PS-$(Im)_2MgBr_2$ > PS-$(Im)_2ZnBr_2$ > PS-$(Im)_2ZnI_2$ > PS-$(Im)_2ZnCl_2$. Thus, the orders of acidity and basicity shown in Fig. 5 are consistent with those derived from CO_2 and NH_3 TPD. In case of different metal containing

PS-$(Im)_2ZnBr_2$ catalysts, the ratio of reaction rate of acetalization to Knoevenagel condensation increased as Zn < Mg < Cu.

3.2. Reactivity of PS-$(Im)_2MX_2$ catalysts

The effects of the molecular structure (different metals and anions) of the PS-$(Im)_2MX_2$ on the synthesis of GC were studied under a vacuum pressure of 14.7 kPa for a reaction time of 6 h at 140 °C; the results are shown in Table 3. In the absence of a catalyst or using MPR alone, the conversion of glycerol was limited to 36% with 45% selectivity toward GC. However, the PS-$(Im)_2MX_2$ catalysts exhibited appreciable activities toward the conversion of glycerol and selectivity of GC. Moreover, a homogeneous catalyst $(HEIm)_2ZnCl_2$ with 1 mol% of glycerol was also tested to compare the reactivity (Table 3). The results indicated that the PS-$(Im)_2MX_2$ catalysts showed higher turnover number (TON) than $(HEIm)_2ZnCl_2$ catalyst even though conversion of glycerol and selectivity of GC remained higher for the $(HEIm)_2ZnCl_2$ catalyst. The catalytic activity of the PS-$(Im)_2MX_2$ catalysts differed depending on the metal and the anion nucleophile. PS-$(Im)_2ZnI_2$ was found to be the most efficient catalyst, with a glycerol conversion of 71.7 and the TON values of 179.6 under the employed reaction conditions. The other catalysts such as PS-$(Im)_2ZnBr_2$ and PS-$(Im)_2ZnCl_2$ were also found active with the TON values of 156.8 and 127.8, respectively. Hence, the order of activity based on the different halide ions followed the order of nucleophilicity: $I^- > Br^- > Cl^-$ **[47,48]**. It is generally accepted that compared to the absolute acidity or basicity, the balance between these two factors plays a more important role in the glycerolysis of urea to GC. As mentioned above, the acidity/basicity ratio of PS-$(Im)_2ZnI_2$ and PS-$(Im)_2ZnBr_2$ is close to unity, whereas that of PS-$(Im)_2ZnCl_2$ is 2.9. Because PS-$(Im)_2ZnI_2$ possesses a greater amount of acid and base sites, this catalyst afforded better activity than PS-$(Im)_2ZnBr_2$. In the case of PS-$(Im)_2MBr_2$ with different metal ions, the Cu-

containing catalyst showed the lowest activity with the lowest TON of 125.3. The results of Table 2 and Fig. 5 suggested that PS-$(Im)_2CuBr_2$ possessed the highest acidity and the highest acidity/basicity ratio. Among the PS-$(Im)_2MBr_2$ catalysts with different metal ions, PS-$(Im)_2ZnBr_2$ exhibited the highest activity (TON of 156.8), possibly because of the subtle balance between its acidity and basicity.

In order to compare the catalytic performance of PS-$(Im)_2MX_2$ with other catalysts, TON of same previously reported catalysts are summarized in Table 3. PS-$(Im)_2ZnI_2$ catalyst has better TON than other previously reported ones except La_2O_3 which is more expensive than this catalyst. Considering the availability and very low price of PS support and zinc halide, and commercial availability of imidazole, this catalyst could be a good candidate for the development of new commercial process for the production of glycerol carbonate.

Despite the apparent simplicity of the reaction of glycerol with urea, this reaction may proceed *via* a large number of possible pathways **[23]**. The accepted mechanism for the reaction involves two steps (Scheme 3): *Step 1*: Carbamoylation of glycerol to 2,3-dihydroxypropyl carbamate (glycerol carbamate) (**3**) with the liberation of an ammonia molecule. This step occurs at a higher reaction rate than the second step. *Step 2*: Carbonylation of the glycerol carbamate to GC (**4**) with the elimination of a second molecule of ammonia **[13]**. Intermediate (**3)** could also produce 4-(hydroxymethyl)oxazolin-2-one (**5**) by a parallel reaction. The produced GC further reacts with urea to form (2-oxo-1,3-dioxolan-4-yl)methyl carbamate (**6**). The presence of specific by-products is important in understanding the effect of the catalyst in the reaction and in elucidating certain of the mechanisms that are operative in the absence or presence of the catalyst. Hence, a set of time-on-line measurements was performed for 8 h to fully identify and quantify all reaction products **[13,23]**, and the results are presented in Fig. 6. The effect of the reaction time on the

synthesis of GC was studied using PS-$(Im)_2ZnI_2$ at 140 °C under a reduced pressure of 14.7 kPa. The ^{13}C NMR profile (Fig. 7) indicates that after 4 h, *ca.* 66.5% of the glycerol was converted, after which the conversion leveled off. The presence of a large amount of (**3**) in the initial stages of the reaction suggests that (**3**) is formed in the first step. However, the selectivity toward the formation of (**3**) decreased after 4 h with a concomitant increase in the selectivity toward GC formation. The selectivity toward the formation of compound (**5**) also decreased in accordance with the trend for (**3**), whereas the concentration of compound (**6**) increased slightly, corresponding to the increasing selectivity toward GC. However, compounds (**5**) and (**6**) were detected in small percentages in comparison to GC.

The FT-IR spectra of the samples taken between 0.5 and 8 h are displayed in Fig. 8. The N=C=O stretching band of isocyanic acid at 2250 cm^{-1} is not present in the spectrum of any of the samples, and thus, the mechanism in which isocyanic acid is produced as the primary product of the reaction can be excluded. This is in agreement with the report by Aresta *et al.* **[22]**, where it was claimed that in the presence of phosphated zirconia catalysts the GC synthesis reaction mechanism does not proceed *via* isocyanic acid as found for $ZnSO_4$; instead, it proceeds *via* 2,3-dihydroxypropyl carbamate (**5**). This is important because the formation of isocyanic acid and its oligomers would represent the undesired transformation of urea. Fig. 8 also shows bands corresponding to urea at 1620 and 1665 cm^{-1} after 2 h of reaction, and the intensity of these bands decreases with time-on-line **[53]**.

Table 4 summarizes the effects of the reaction temperature on the synthesis of GC in the presence of PS-$(Im)_2ZnI_2$. The conversion of glycerol continuously increased as the temperature increased from 100 to 160 °C. The selectivity toward GC increased with temperature, reaching a maximum of 84.1% for PS-$(Im)_2ZnI_2$ at 140 °C; however, the selectivity decreased sharply when the temperature exceeded 150 °C. The ^{13}C NMR (Fig. 9)

[22,23] and FT-IR (Fig. 10) **[23,53]** profiles show that the intensity of the peaks at 77.5 ppm in the NMR spectrum and at 1730 cm^{-1} in the FT-IR spectrum, corresponding to compound (**5**), increased above 140 °C and the selectivity of (**5**) increased to 16.7% at 160 °C. Moreover, based on the ^{13}C NMR peak at 71.2 ppm, it was found that an unidentified product was also detected, corresponding to 64.6% selectivity at 160 °C, which can be attributed to the polymerization of GC and/or glycerol that has not yet been well characterized **[54]**. The formation of polymers from GC or glycerol has been reported to be one of the main factors responsible for the low selectivity toward GC **[13]**.

The effects of the degree of vacuum on the reactivity of the PS-$(Im)_2ZnI_2$ catalyst are presented in Table 5. The conversion of glycerol increased as the degree of vacuum increased from 101.3 to 3.1 kPa. Application of a high degree of vacuum could enhance the removal of the generated ammonia gas, thereby accelerating the forward reaction of glycerol and urea. The selectivity toward GC also appeared to follow a similar trend with an increase in the applied vacuum from 101.3 to 1.1 kPa, because a high degree of vacuum may increase the conversion of compound (**3**) to GC. Interestingly, removal of ammonia by nitrogen purging at a flow rate of 150 mL/min was also effective for the glycerolysis of urea, resulting in 73.8% glycerol conversion and 61.8% GC yield using PS-$(Im)_2ZnI_2$ under the same reaction conditions as used above.

The effect of the catalyst loading on the yield of GC was investigated using PS-$(Im)_2ZnI_2$ at 140 °C for 6 h with a vacuum pressure of 14.7 kPa. As shown in Table 6, the yield of GC and the glycerol conversion increased continuously as the catalyst loading increased up to 5 wt%. However, the yield remained almost constant on increasing the catalyst loading to 10 and 15 wt%. Therefore, 5 wt% can be considered as the optimum amount of catalyst in this work.

The effect of the reactant ratio (glycerol/urea) on the activity of PS-$(Im)_2ZnI_2$ was evaluated by keeping the reaction parameters constant while varying the initial amount of urea; the results are summarized in Table 7. Increasing the glycerol/urea molar ratio had the obvious consequence of reducing the glycerol conversion because sufficient urea is not present, which makes urea the limiting reactant. Thus, with a glycerol to urea ratio of 0.5, only 45.0% glycerol conversion was achieved out of a maximum possible conversion of 50%, whereas in the presence of more urea, 75.5% conversion was achieved. More importantly, the selectivity of the reaction changed gradually with variations of the molar ratio of the two reactants. In particular, the selectivity toward GC decreased from 90.2% (at a glycerol to urea ratio of 2) to 38.5% (at a glycerol to urea ratio of 0.5). Furthermore, increasing the urea concentration enhanced the consecutive carbonylation reaction producing (**6**), and the selectivity toward (**6**) increased from 0.6% to 11.4%.

The stability of the PS-$(Im)_2ZnI_2$ catalyst was evaluated in recycling experiments. For each cycle, the used catalyst was separated by filtration, washed with methanol to remove the products adhering to the surface of the catalyst, dried at room temperature, and then reused directly for the next run without regeneration. The activity of the reused PS-$(Im)_2ZnI_2$ catalyst is summarized in Table 8. Although the conversion of glycerol decreased slightly with the catalyst used over three cycles, the selectivity toward GC was almost the same as achieved with the fresh catalyst. To determine whether the active $(Im)_2MX_2$ center underwent any leaching from the immobilized polystyrene, FT-IR analysis of the fresh PS-$(Im)_2ZnI_2$ catalyst and that used for three cycles was performed (Fig. 11). The characteristic peaks of the PS-$(Im)_2ZnI_2$ were similarly presented for the recycled and fresh catalysts. The XPS spectra of the fresh PS-$(Im)_2ZnI_2$ and that used for three cycles (Fig. 12) demonstrated the similarity of the spectra of the recycled and fresh catalysts. The peak at 401.7 eV

corresponding to the imidazolium nitrogen and those of I^- remained intact, even though the intensities decreased slightly. Therefore, it can be concluded that the PS-$(Im)_2ZnI_2$ catalyst could be recycled up to three consecutive cycles without any considerable loss of its initial activity. In order to check a possible contribution of a homogeneous catalytic action of active $(Im)_2ZnI_2$ leached into solution, hot catalyst filtration test was performed after 3 h of reaction. As shown in Fig. 6, no further glycerol yield in the filtrate occurred after catalyst removal at the reaction temperature, indicating that catalysis is not due to the soluble homogeneous species.

4. Conclusions

The polymer supported metal containing ionic liquid catalysts based on imidazolium, PS-$(Im)_2MX_2$, were successfully synthesized and characterized by various physicochemical methods. The PS-$(Im)_2MX_2$ catalysts showed good catalytic activity for the synthesis of GC from urea and glycerol under mild reaction conditions. Among the PS-$(Im)_2MBr_2$ catalysts, the best catalytic performance was achieved with PS-$(Im)_2ZnBr_2$ since Zn containing catalyst had better acid/base ratio than Mg and Cu containing ones. PS-$(Im)_2ZnI_2$ with well-balanced acid-base properties exhibited the best catalytic activity, because the Lewis-acid sites activate the carbonyl groups of urea and the Lewis-base sites activate the hydroxyl groups of the glycerol. The catalyst was also easily recovered and reused without any considerable loss of the initial activity.

Acknowledgements

This study was supported by the Ministry of Education of Korea through National Research Foundation (2012-001507), Global Frontier program, and KBSI.

References

[1] G. Knothe, J. Van Gerpen, J. Krahl (Eds.), The Biodiesel Handbook, AOCS Press, Champaign, Illinois, 2005.

[2] S.T. Bagley, L.D. Gratz, J. Johnson, J. McDonald, Environ. Sci. Tech. 32 (1998) 1183-1191.

[3] M. Mittelbach, C. Remschmidt, Biodiesel-The Comprehensive Handbook, Graz, Austria, 2004.

[4] T. Werpy, G. Petersen, Top value added chemicals from biomass, Vol. 1, US Department of Energy (USDOE), 2004.

[5] A.S. Kovvali, K.K. Sirkar, Ind. Eng. Chem. Res. 41 (2002) 2287-2295.

[6] J. Rousseau, C. Rousseau, Tetrahedron 65 (2009) 8571-8581.

[7] M. Selva, M. Fabris, Green Chem. 11 (2009) 1161-1172.

[8] M. Ghandi, A. Mostashari, M. Karegar, M.J. Barzegar, Am. Oil Chem. Soc. 84 (2007) 681-685.

[9] G. Rokicki, P. Rokoczy, P. Parzuchowski, M. Sobiecki, Green Chem. 7 (2005) 529-539.

[10] V. Plasman, T. Caulier, N. Boulos, Plast. Addit. Compd. 7 (2005) 30-33.

[11] M.O. Sonnati, S. Amigoni, E.P.T. Givenchy, T. Darmanin, O. Choulet, F. Guittard, Green Chem. 15 (2013) 283-306.

[12] Y. Fukuda, Y. Yamamoto, JP No. 023930 (2009).

[13] M.J. Climent, A. Corma, P.D. Frutos, S. Iborra, M. Noy, A. Velty, P. Concepcion, J. Catal.

269 (2010) 140-149.

[14] Z. Mouloungui, J.W. Yoo, C.A. Gachen, A. Gaset, EP No. 0739888 (1996).

[15] M. Aresta, A. Dibenedetto, F. Nocito, C. Pastore, J. Mol. Catal. A: Chem. 257 (2006) 149-153.

[16] Q. Li, W. Zhang, N. Zhao, W. Wei, Y. Sun, Catal. Today 115 (2006) 111-116.

[17] M. Okutsu, T. Kitsuki, JP No. 039347 (2007).

[18] M. Aresta, J. L. Dubois, A. Dibenedetto, F. Nocito, C. Ferragina, EP No. 08305653.1 (2008).

[19] T. Sasa, M. Okutsu, M. Uno, JP No. 067689 (2009).

[20] M. Okutsu, T. Kitsuki, JP No. 050415 (2000).

[21] S. Fujita, Y. yamanishi, M. Arai, J. Catal. 297 (2013) 137-141.

[22] M. Aresta, A. Dibenedetto, F. Nocito, C. Ferragina, J. Catal. 268 (2009) 106-114.

[23] C. Hammond, J.A.L. Sanchez, M.H.A. Rahim, N. Dimitratos, R.L. Jenkins, A.F. Carley, Q. He, C.J. Kiely, D.W. Knight, G.J. Hutchings, Dalton Trans. 40 (2011) 3927-3937.

[24] N.E. Leadbeater, M. Marco, Chem. Rev. 102 (2002) 3217-3274.

[25] C.A. McNamara, M.J. Dixon, M. Bradley, Chem. Rev. 102 (2002) 3275-3300.

[26] S. Bhattacharyya, Com. Chem. High Throughput Screen. 3 (2000) 65-92.

[27] G.R. Krishnan K. Sreekumar, Appl. Catal. A: Gel. 353 (2009) 80-86.

[28] J. Sun, W. Cheng, W. Fan, Y. Wang, Z. Meng S. Zhang, Catal. Today 148 (2009) 361-367.

[29] C. Qi, J. Ye, W. Zang H. Jiang, Adv. Synth. Catal. 352 (2010) 1925-1933.

[30] D.W. Kim, M.S. Park, M. Selvaraj, G.A. Park, S.D. Lee, D.W. Park, Res. Chem. Intermed. 37 (2011) 1305-1312.

[31] J.H. Park, J.S. Choi, S.K. Woo, S.D. Lee, M. Cheong, H.S. Kim, H. Lee, Appl. Catal. A: Gen. 433 (2012) 35-40.

[32] P. Ball, H. Fullmann, W. Heitz, Angew. Chem. Int. Ed. Engl. 19 (1980) 718-720.

[33] D.W. Kim, D.W. Park, J. Nanosci. Nanotechno. (2013) in press.

[34] C.K. Lee, M.J. Ling, I.J.B. Lin, Dalton Tran. 24 (2003) 4731-4737.

[35] J.I. Yu, H.J. Choi, M. Selvaraj, D.W. Park, React. Kinet. Mech. Cat. 102 (2011) 353-365.

[36] A. Chowdhury, S. T. Thynell, Thermochim. Acta. 443 (2006) 159-172.

[37] I. Niedermaier, C. Kolbeck, N. Taccardi, P.S. Schulz, J. Li, T. Drewello, P. Wasserscheid, H.P. Steinruck, F. Maier, Chem. Phys. Chem. 13 (2012) 1725-1735.

[38] J. Tharun, Y.S. Hwang, R. Roshan, S.H. Ahn, A.C. Kathalikkattil, D.W. Park, Catal. Sci. Technol. 2 (2012) 1674-1680.

[39] A.C. Kathalikkattil, J. Tharun, R. Roshan, H.G. Soek, D.W. Park, Appl. Catal. A: Gen. 447 (2012) 107-114.

[40] N. Vallapa, O. Wiarachai, N. Thongchul, J. Pan, V. Tangpasuthadol, S. Kiatkamjornwong, V. P. Hoven, Carbohydr. Polym. 83 (2011) 868-975.

[41] D. Derouet, S. Forgeard, J.C. Brosse, J. Emery, J.Y. Buzare, J. Polym. Sci. Pol. Chem. 36 (1998) 437-453.

[42] B. Yu, F. Zhou, C. Wang, W. Liu, Eur. Poly. J. 43 (2007) 2699-2707.

[43] J. Kim, S.N. Kim, H.G. Jang, G. Seo, W.S. Ahn, Appl. Catal. A: Gen. 453 (2013) 175-180.

[44] G. Jiang, L. Zhang, Z. Zhao, X. Zhou, A. Duan, C. Xu, J. Gao, Appl. Catal. A: Gen. 340 (2008) 176-182.

[45] M. Kotke, P.R. Schreiner, Tetrahedron 62 (2006) 434-439.

[46] T.S. Jin, J.S. Zhang, A.Q. Wang, T.S. Li, Synthetic Commun. 34 (2004) 2611-2616.

[47] J. Sun, S. Fujita, F. Zhao, M. Arai, Green. Chem. 6 (2004) 613-616.

[48] J.I. Yu, H.Y. Ju, K.H. Kim, D.W. Park, Korean J. Chem. Eng. 27 (2010) 446-451.

[49] S.D. Lee, K.A. Park, D.W. Kim, D.W. Park, J. Nanosci. Nanotechno. (2013) accepted.

[50] S. Claude, Z. Mouloungui, J.W. Yoo, A. Gaset, US No. 6025504 (2000).

[51] M. Okutsu, T. Kitsuki, US No. 6495703 (2002).

[52] L. Wang, Y. Ma, Y. Wang, S. Liu, Y. Deng, Catal. Commun. 12 (2011) 1458-1462.

[53] V.C. Casilda, G. Mul, J.F.Fernandez, F.R. Marcos, M.A. Banares, Appl. Catal. A: Gen. 409 (2011) 106-112.

[54] A. Dibenedetto, F. Nocito, A. Angelini, I. Papai, M. Aresta, R. Mancuso Chem. Sus. Chem. 6 (2013) 345-352.

Table 1 Elemental analysis results of PS-$(Im)_2MX_2$.

Catalyst	CNO from elemental analysis			Amount of $(Im)_2MX_2$[a] (mmol/g)
	C (wt%)	N (wt%)	O (wt%)	
PS-$(Im)_2ZnCl_2$	77.57	3.34	1.44	0.60
PS-$(Im)_2ZnBr_2$	63.88	3.68	2.41	0.66
PS-$(Im)_2ZnI_2$	53.43	4.11	3.69	0.73
PS-$(Im)_2MgBr_2$	68.20	4.23	5.12	0.76
PS-$(Im)_2CuBr_2$	61.64	5.01	3.74	0.89

[a]Amount of metal containing imidazolium salt immobilized onto Merrifield's peptide resin

Table 2 The amount of acid and base in CO_2- and NH_3-TPD of PS-$(Im)_2MX_2$.

Catalyst	CO_2-TPD (mmol/g)			NH_3-TPD (mmol/g)			A/B[e]
	Weak base[a]	Strong base[b]	total	Weak-medium acid[c]	Strong acid[d]	total	
PS-$(Im)_2ZnCl_2$	1.22	0.79	2.01	1.85	4.00	5.85	2.9
PS-$(Im)_2ZnBr_2$	3.47	0.32	3.79	3.79	0.39	4.18	1.1
PS-$(Im)_2ZnI_2$	4.50	2.17	6.67	3.18	2.83	6.01	0.9
PS-$(Im)_2MgBr_2$	2.61	1.31	3.92	7.92	6.97	14.89	3.8
PS-$(Im)_2CuBr_2$	2.05	1.75	3.80	45.49	6.41	41.90	11.1

[a] 323 ~ 423 K.
[b] 423 ~ 573 K.
[c] 323 ~ 523 K.
[d] 473 ~ 573 K.
[e] Acid/base ratio

Table 3 The reactivity of PS-$(Im)_2MX_2$ and in the glycerolysis of urea.

Catalyst	X_G (%)	S_{GC} (%)	Y_{GC} (%)	TON[a]	Ref.
Blank	34.4	44.5	15.3	-	This work
MPR	36.4	43.1	15.7	-	This work
PS-$(Im)_2ZnCl_2$	61.2	57.7	35.3	127.8	This work
PS-$(Im)_2ZnBr_2$	65.8	72.3	47.6	156.8	This work
PS-$(Im)_2ZnI_2$	71.7	84.1	60.3	179.6	This work
PS-$(Im)_2MgBr_2$	67.9	73.9	50.7	145.0	This work
PS-$(Im)_2CuBr_2$	62.5	72.1	51.3	125.3	This work
$(HEIm)_2ZnCl_2$	92.7	93.4	86.6	86.6	[33]
TBABr	51.0	60.4	30.8	61.6	[49]
PS-SO_3Mg	-	-	58	35.0	[50]
MgO	73.0	53.0	39.0	3.4	[13]
$ZnCl_2$	84.0	97.0	81.5	22.1	[21]
ZnO	62.0	93.0	58.0	5.9	[51]
$MgSO_4$	72.0	92.0	66.0	8.0	[51]
La_2O_3	69.0	98.0	68.0	374.0	[52]

Reaction conditions: Glycerol / Urea = 1, Cat./glycerol = 5 wt%, Temp. = 140 °C, Degree of vacuum = 14.7 kPa, Reaction time = 6 h.

[a]TON=(mole of GC)/(mole of catalyst)

Table 4 The effect of reaction temperature on the reactivity of PS-$(Im)_2ZnI_2$.

Reaction Temp. (°C)	X_G%	S_{GC}%	$S_{(3)}$%	$S_{(5)}$%	$S_{(6)}$%	$S_{(U)}$%[a]	Y_{GC}%
100	16.3	19.2	-	-	-	-	3.1
110	20.6	20.3	-	-	-	-	4.2
120	33.7	25.9	-	-	-	-	8.7
130	58.1	42.6	-	-	-	-	24.8
140	71.7	84.1	8.1	1.1	4.2	-	60.3
150	78.3	68.3	7.5	10.6	6.2	5.5	53.5
160	85.0	5.1	6.9	16.7	-	64.6	4.3

Reaction conditions: Glycerol / Urea = 1, Cat./glycerol = 5 wt% PS-$(Im)_2ZnI_2$, Degree of vacuum = 14.7 kPa, Reaction time = 6 h.

[a] $S_{(u)}$ is selectivity of unidentified by product showing ^{13}C NMR peak at 79.2 ppm

Table 5 The effect of degree of vacuum on the reactivity of PS-$(Im)_2ZnI_2$.

Degree of vacuum (kPa)	X_G%	S_{GC}%	Y_{GC}%
3.1	74.9	85.7	64.3
14.7	71.7	84.1	60.3
27.9	67.5	71.5	48.3
54.3	51.5	69.8	36.0
101.3	43.6	63.0	27.5
150 mL N_2 purge	73.8	83.7	61.8

Reaction conditions: Glycerol / Urea = 1, Cat./glycerol = 5 wt% PS-$(Im)_2ZnI_2$, Temp. = 140 °C, Reaction time = 6 h.

Table 6 The effect of catalyst amount on the reactivity of PS-$(Im)_2ZnI_2$.

Amount of Catalyst (wt%)	X_G (%)	S_{GC} (%)	Y_{GC} (%)
1	50.8	77.0	39.1
2	59.5	76.8	45.7
3	66.0	80.6	53.2
5	71.7	84.1	60.3
10	72.4	82.3	59.6
15	73.0	83.4	60.9

Reaction conditions: Glycerol / Urea = 1, Cat./glycerol = x wt% PS-$(Im)_2ZnI_2$, Temp. = 140 °C, Degree of vacuum = 14.7 kPa, Reaction time = 6 h.

Table 7 The effect of the ratio of glycerol/urea on the reactivity of PS-$(Im)_2ZnI_2$.

Glycerol / Urea	X_G%	S_{GC}%	$S_{(3)}$%	$S_{(5)}$%	$S_{(6)}$%	Y_{GC}%
0.5	75.5	38.5	36.9	9.4	14.1	29.1
1	71.7	84.1	8.1	1.1	4.2	60.3
2	45.0	90.2	1.9	1.0	0.6	40.6

Reaction conditions: Cat./glycerol = 5 wt% PS-$(Im)_2ZnI_2$, Temp. = 140 °C, Degree of vacuum = 14.7 kPa, Reaction time = 6 h.

Table 8 Recycle test of PS-$(Im)_2ZnI_2$.

	X_G%	S_{GC}%	Y_{GC}%
Fresh	71.7	84.1	60.3
1^{st}	70.1	82.7	58.0
2^{nd}	65.7	81.1	53.3
3^{rd}	56.6	82.1	46.5

Reaction conditions: Glycerol / Urea = 1, Cat./glycerol = 5 wt% PS-$(Im)_2ZnI_2$, Temp. = 140 °C, Degree of vacuum = 14.7 kPa, Reaction time = 6 h.

List of scheme and figures

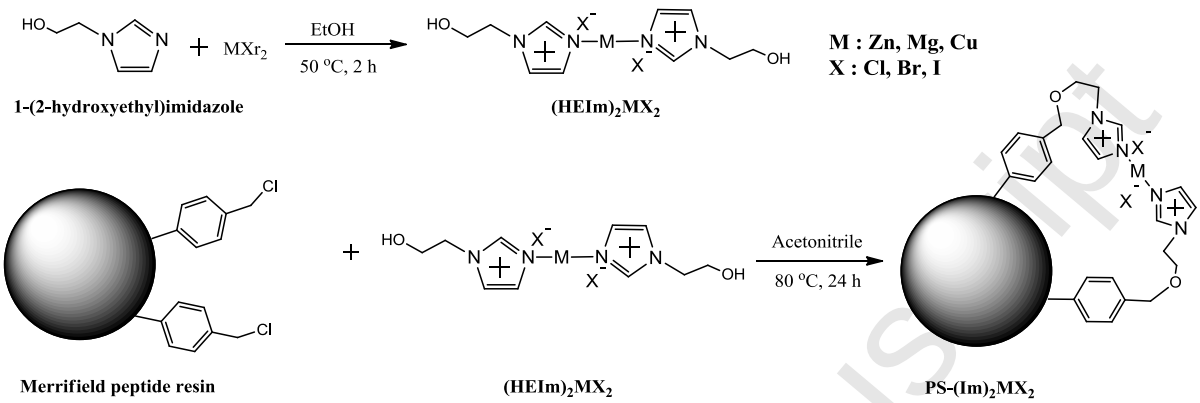

Scheme 1. Preparation of polystyrene-supported metal containing imidazolium salt catalyst

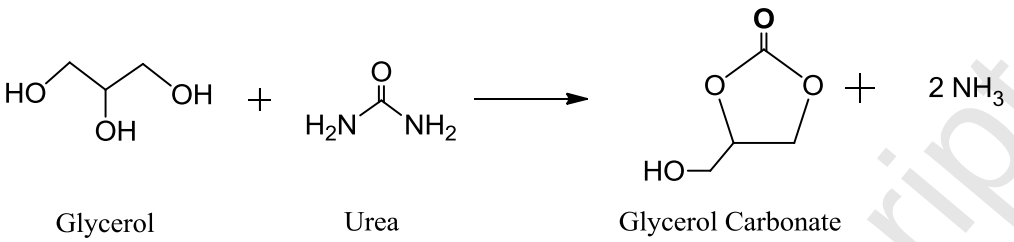

Scheme 2. Synthesis of glycerol carbonate by glycerolysis of urea

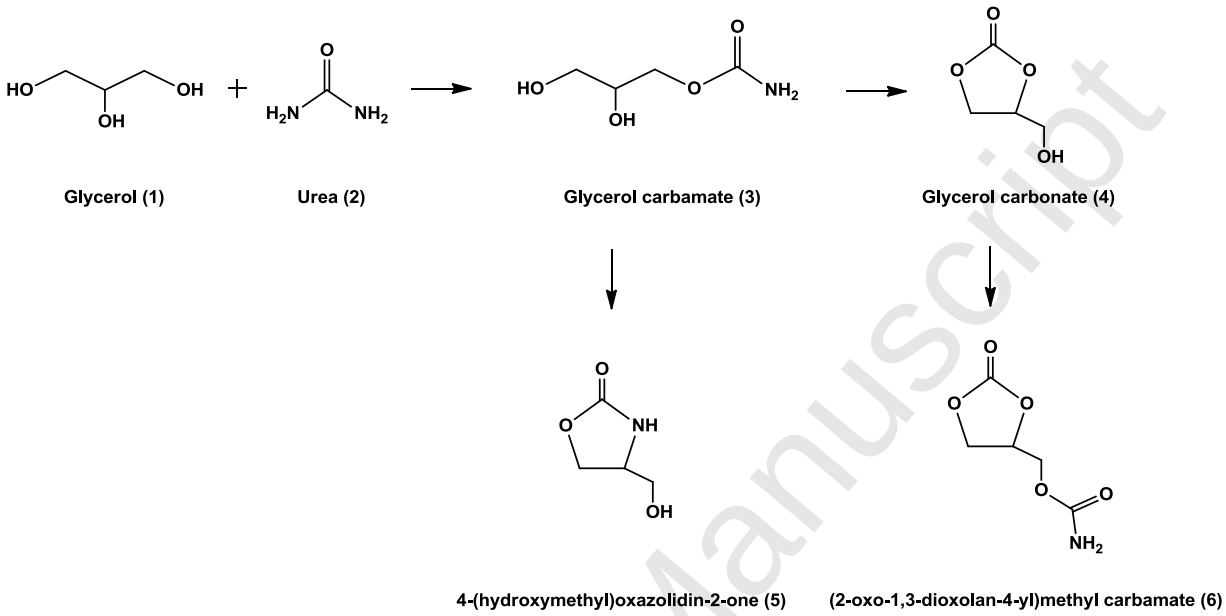

Scheme 3. Possible reaction pathways for the glycerolysis of urea

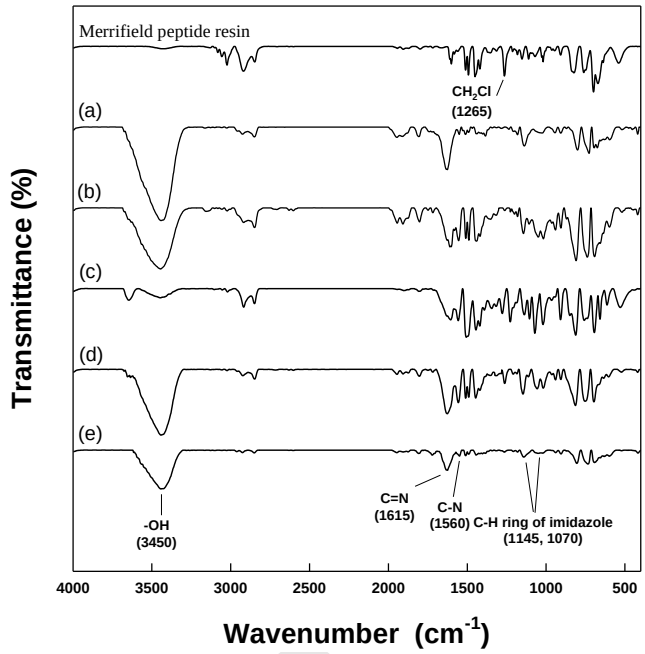

Fig. 1. FT-IR spectra of PS-$(Im)_2MX_2$ and Merrifield peptide resin: (a) PS-$(Im)_2ZnI_2$, (b) PS-$(Im)_2ZnBr_2$, (c) PS-$(Im)_2ZnCl_2$, (d) PS-$(Im)_2MgBr_2$, (e) PS-$(Im)_2CuBr_2$.

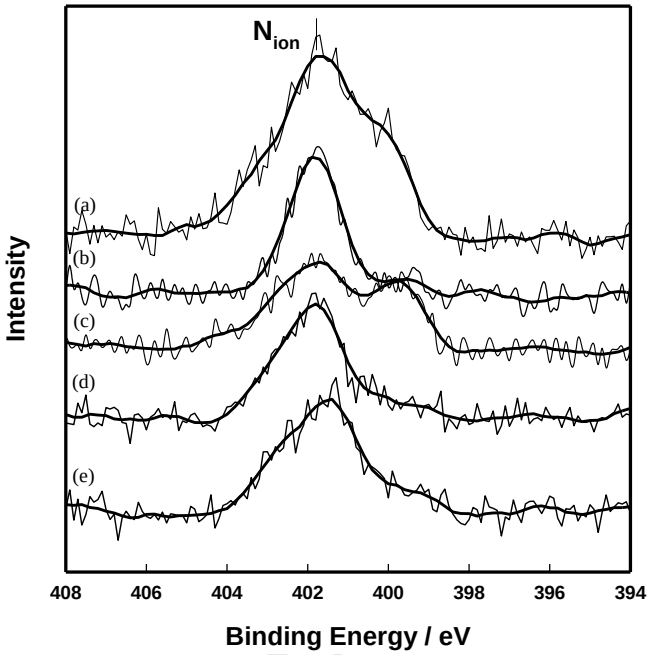

Fig. 2. N 1s XPS spectra of PS-$(Im)_2MX_2$: (a) PS-$(Im)_2ZnI_2$, (b) PS-$(Im)_2ZnBr_2$, (c) PS-$(Im)_2ZnCl_2$, (d) PS-$(Im)_2MgBr_2$, (e) PS-$(Im)_2CuBr_2$

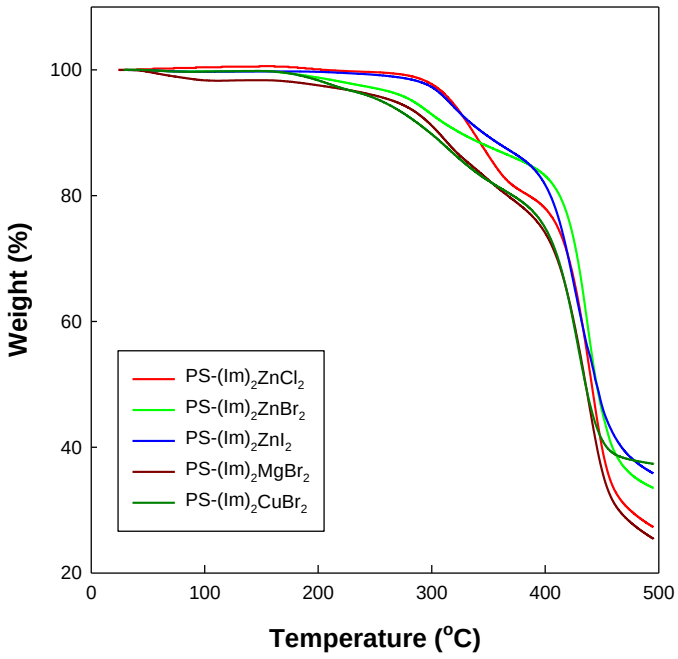

Fig. 3. TGA results of PS-$(Im)_2MX_2$

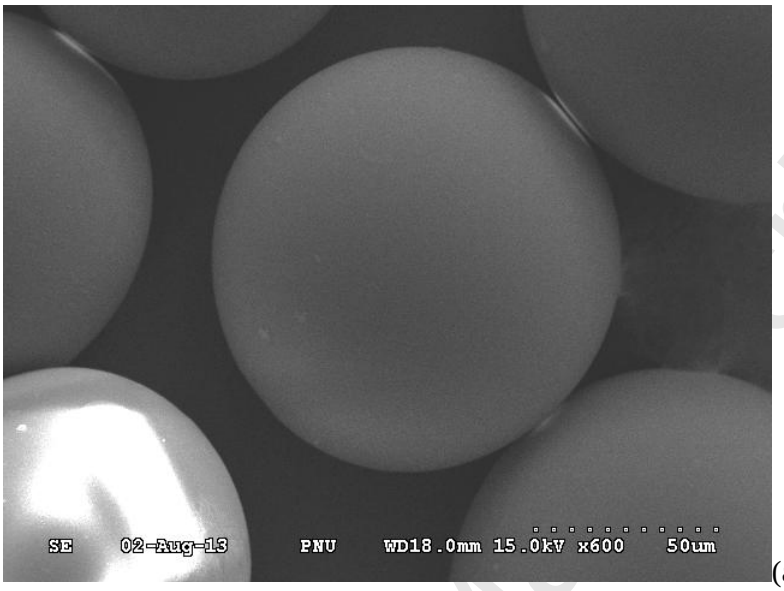

(a)

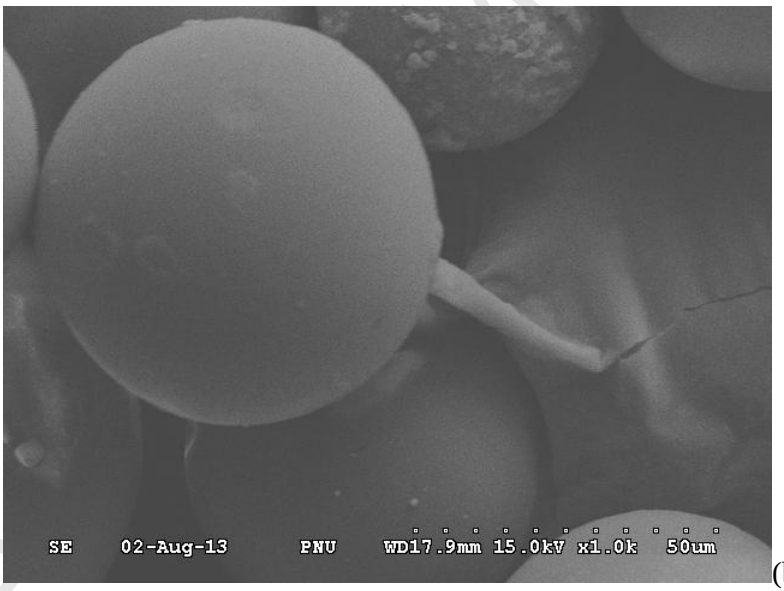

(b)

Fig. 4. SEM image of (a) Merrifield's peptide resin and (b) PS-$(Im)_2ZnI_2$

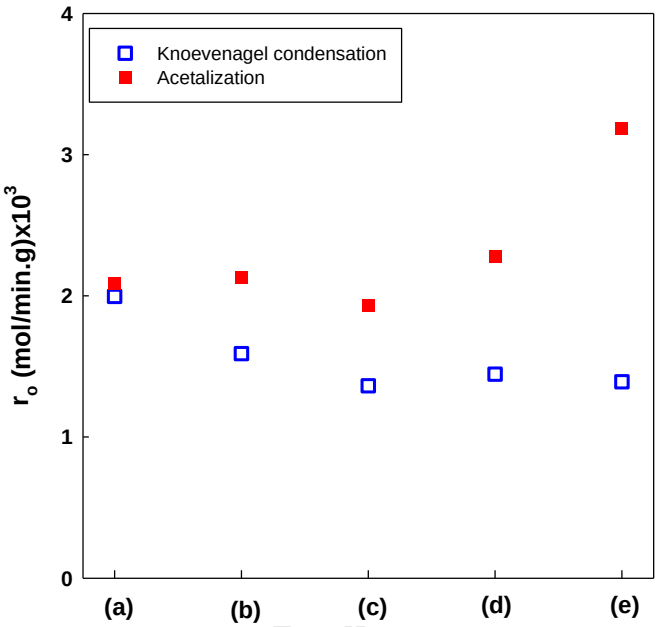

Fig. 5. Relatives between acidity and basicity of PS-$(Im)_2MX_2$: (a) PS-$(Im)_2ZnI_2$, (b) PS-$(Im)_2ZnBr_2$, (c) PS-$(Im)_2ZnCl_2$, (d) PS-$(Im)_2MgBr_2$, (e) PS-$(Im)_2CuBr_2$.

[Conditions: Knoevenagel condensation - 10 mmol of benzaldehyde and 10 mmol of malononitrile (1 wt% of cat., room temp.), Acetalization of 10 mmol of benzaldehyde with 20 mmol of EtOH (1 wt% of cat., 60 °C)]

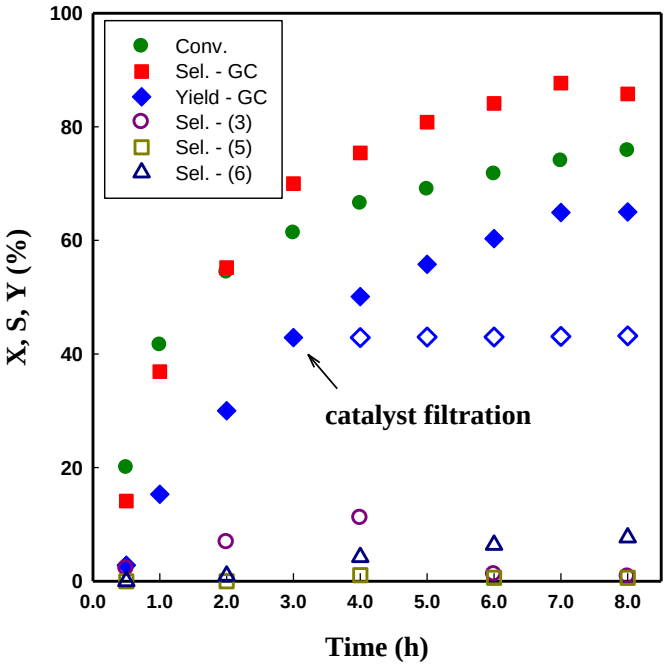

Fig. 6. Time variant conversion, yield, and selectivities of products

[Conditions: Glycerol / Urea = 1, Cat./glycerol = 5 wt%, Temp. = 140 °C, Degree of vacuum = 14.7 kPa, ◇: GC yield after catalyst filtration]

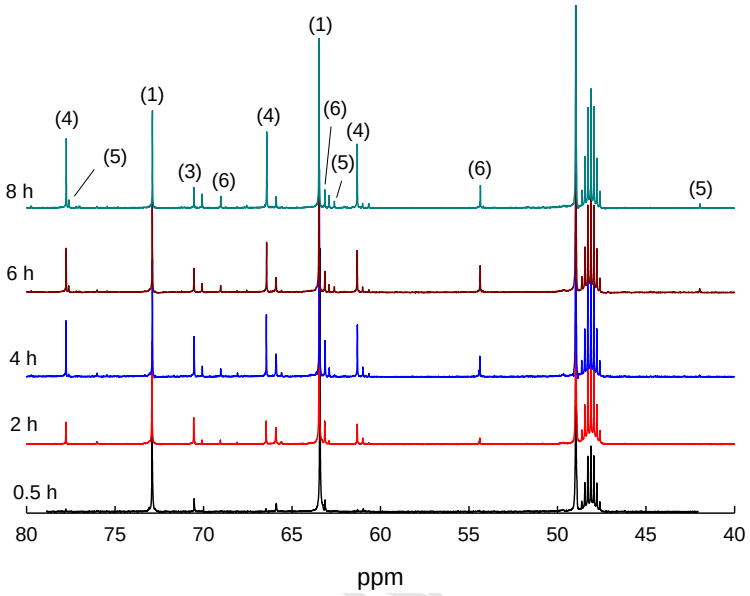

Fig. 7. ^{13}C NMR spectra of reaction mixtures by during the reaction with PS-$(Im)_2ZnI_2$

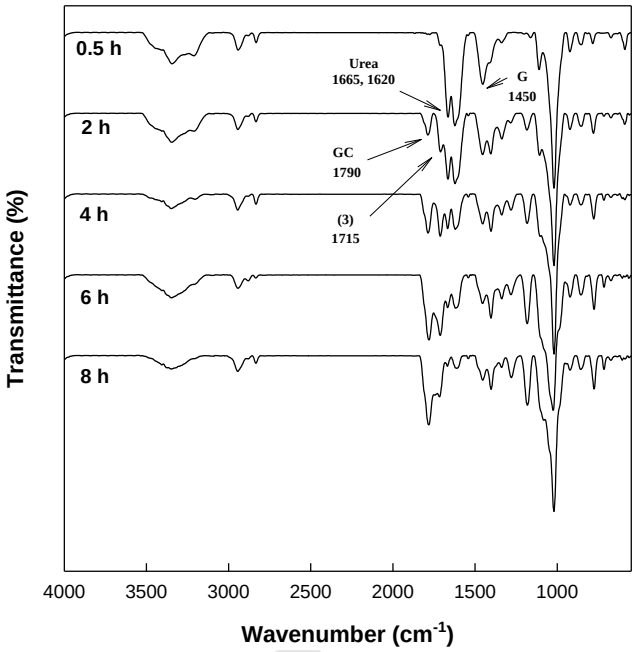

Fig. 8. FT-IR spectra of reaction mixtures during the reaction with PS-$(Im)_2ZnI_2$

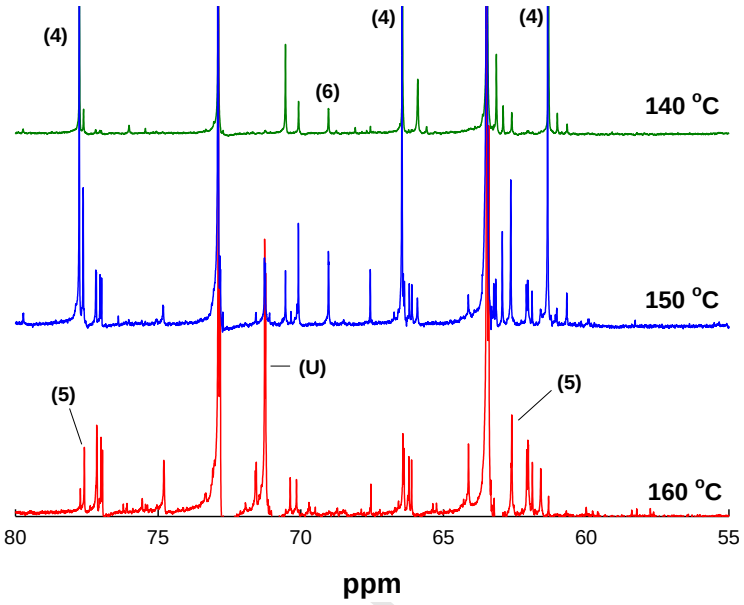

Fig. 9. . ^{13}C NMR spectra of reaction mixtures at different temperature with PS-$(Im)_2ZnI_2$

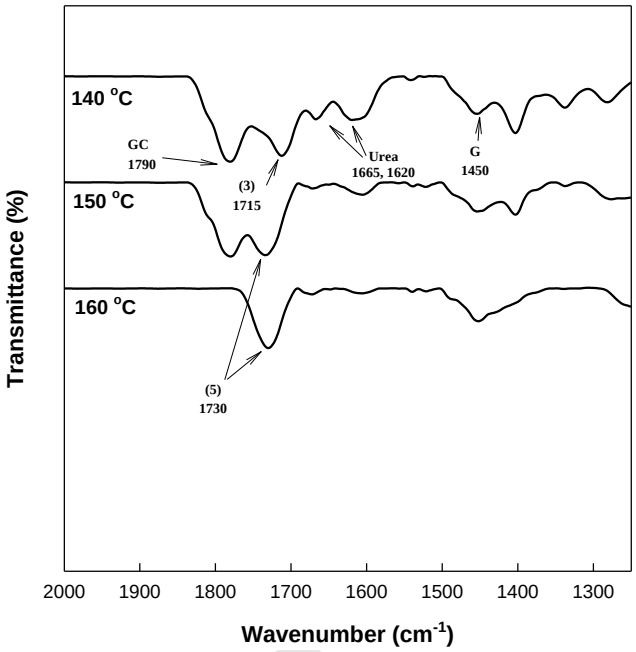

Fig. 10. FT-IR spectra of reaction mixtures at different temperature with PS-$(Im)_2ZnI_2$

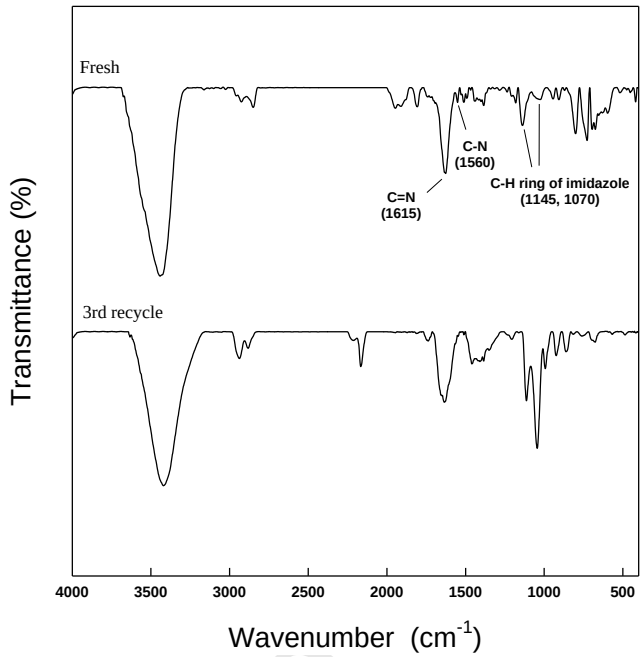

Fig. 11. FR-IR spectra of fresh and 3rd reused PS-$(Im)_2ZnI_2$

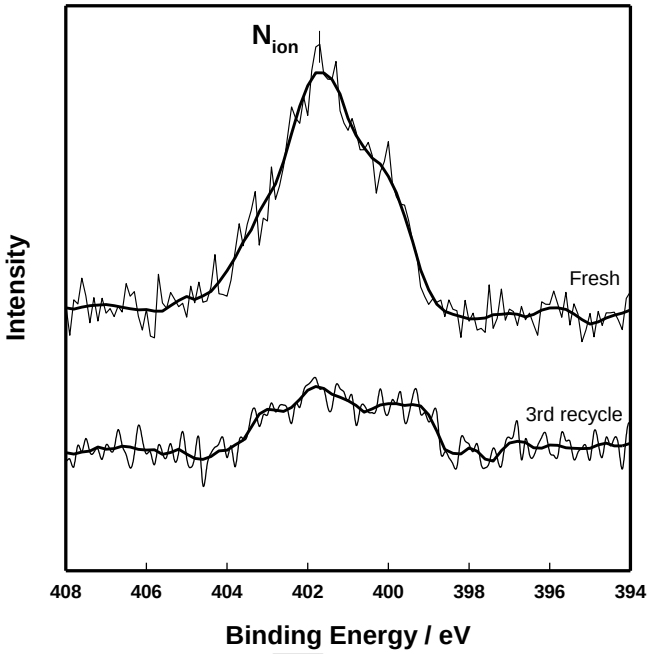

Fig. 12. N 1s XPS spectra of fresh and 3rd reused PS-$(Im)_2ZnI_2$